Experimental analysis and predictive modelling of Ti6Al4V laser surface texturing for biomedical applications

Francisca Melo-Fonseca [a,b,c,*], Bruno Guimarães [a,b], Michael Gasik [d,e], Filipe S. Silva [a,b,1], Georgina Miranda [f,1]

[a] Center for MicroElectroMechanical Systems (CMEMS-UMinho), University of Minho, Campus de Azurém, 4800-058 Guimarães, Portugal
[b] LABBELS – Associate Laboratory, Braga, Guimarães, Portugal
[c] International Iberian Nanotechnology Laboratory (INL), 4715-330 Braga, Portugal
[d] School of Chemical Engineering, Aalto University Foundation, FI-00076 Espoo, Finland
[e] Several Ltd., Helsinki, Finland
[f] CICECO, Aveiro Institute of Materials, Department of Materials and Ceramic Engineering, University of Aveiro, 3810-193 Aveiro, Portugal

ARTICLE INFO

ABSTRACT

Laser surface texturing (LST) is a powerful technique for creating high quality micro-textured patterns with different shapes and sizes on metallic biomaterials. Textured surfaces may improve the interaction between bone and implant by increasing the surface contact area and thus promoting bone regeneration. The goal of this study was to explore Nd:YAG laser potential for texturing micro-scale pillars with pyramid geometry, with dimensions in a selected range, in a reproducible way. First, the design and texture of grooves were addressed, then proceeding to pillars. Two laser machining and marking strategies were investigated, and the consecutive laser processing strategy and continuous marking mode were selected due to the resultant smoother grooves. Then, a cross-hatched pattern was designed to texture a pillar pattern with targeted dimensions. Given the direct effect of the LST drawing and laser parameters on the texture dimensions, three mathematical models, one for each texture dimension (groove width, pillar width and pillar depth) were developed. These models are accurate tools for predicting the texture dimensions in the selected range and this LST approach was effective on creating well-defined, uniform and equally spaced surface textures on Ti6Al4V parts, in a reproducible way. A combination of drawing and laser parameters was selected for the target dimensions, also considering suitable wettability and roughness for biomedical applications.

1. Introduction

Metallic materials are widely used for dental and orthopaedic applications, specially titanium (Ti) and Ti-based materials, which are considered the number one choice due to a combination of corrosion resistance, fatigue strength, low Young's modulus amongst metals and alloys and biocompatibility [1–3]. Nevertheless, in order to improve the interaction between bone and implant, a broad set of surface treatments have been subject of great interest. These range from simple use of 2D materials, such as protective coatings, and the creation of porous structures to more complex processes, such as fabrication of textured surfaces [4,5]. More examples can be found in previous review studies on this matter [4,6,7]. Wang et al. added a protective coating on Ti alloys by anodization, which exhibited a lower contact angle, higher roughness and similar cell viability compared to untreated Ti alloy [8]. The hydrothermal treatment was proposed as capable of creating a potentially bioactive and hydrophilic layer on Ti able to enhance the bone-implant interface [9]. Henningsen et al. investigated the potential of UV light and non-thermal plasma treatment of argon and oxygen on Ti surfaces and concluded that, after short-term functionalization, both techniques improved the surface properties and cellular response [10]. Another strategy is the fabrication of specific patterns on the implant's surface which, besides increasing the surface contact area, may improve some properties and performance, as wetting, tribological or biological behaviour [11–13]. In fact, cell-substrate adhesion is influenced by substrate topography and the impact of topographical features on

---

* Corresponding author.
  E-mail address: franciscarmelofonseca@gmail.com (F. Melo-Fonseca).
[1] Co-last authorship.

cellular response and behaviour has been covered in the literature [14,15].

One of the most promising surface modification processes is the laser surface texturing (LST) due to its high beam quality, high efficiency, accuracy, flexibility, precision and environmental-friendliness [16]. Surface texturing obtained through the action of a laser consists in the incidence of a high-energy beam on the material surface, generating melting and vaporization of the material from the irradiated area [17]. Although this non-conventional machining process allows a good control of micro-textured patterns shape and size, Ding et al. had shown that the final surface topographies are strongly dependent on the laser parameters including the laser wavelength, pulse duration, frequency and laser power [18].

The Q-switched Nd:YAG laser technology has been used to produce a variety of textures such as microchannels [19], grooves [20], holes [21,22] and pillars [23] on Ti-based materials. Topological features have been shown to influence the cellular response and therefore have a potential use for biomedical applications. Therefore, surface texturing has been investigated to enhance the antimicrobial properties and osseointegration to improve the long-term performance of metallic biomaterials [7,11]. Lawrence et al. used Nd:YAG laser to alter the surface properties of Ti6Al4V and concluded that by increasing the wettability as a result of an increased surface roughness, surface oxygen content and polar component of the surface energy, osteoblast cell activity was improved [24]. A groove pattern (20 and 60 μm width and 2 μm depth) was created on Ti6Al4V using a femtosecond laser and mesenchymal stem cells (MSC) aligned in the grooves direction and produced cytoplasmic extensions with focal contacts [25]. In another study, micro-grooves were fabricated using a combination of photolithography and inductively coupled plasma-based dry etching on Ti substrate with varying dimensions (groove width of 7 and 12 μm, ridge width of 3 and 10 μm and depth of 2 μm). These patterns enhanced the in vitro osteogenic differentiation of MC3T3-E1 preosteoblastic cells and the pattern with groove width of 7 μm and ridge of 3 μm presented the strongest contact guidance and could effectively stimulate the in vivo bone regeneration [26]. Tiainen et al. developed cross-hatched micropatterns on Ti6Al4V (varying groove width of 40, 80 and 140 um and groove spacing of 0, 20 and 100 μm) which wettability behaviour and structural stability were evaluated, the latter by friction tests against bone [27]. In a different study, laser-induced periodic surface structures (LIPSS) and nanopillars were produced by a femtosecond laser on Ti grade 2 and both laser patterns reduced the biofilm formation and bacterial adhesion, therefore reducing the risk of implant-associated infections [28]. Luo et al. used a femtosecond laser to produce nano-ripples on Ti6Al4V capable of preventing biofilm formation and bacterial adhesion, while promoting proliferation of rat MSC [29].

For the purpose of, for example, total joint replacements, surface texturing may be tailored not only to improve the biological interaction of the biomaterial but also the tribological performance, which can be improved by enhancing lubrication and wear resistance [30,31]. However, texture dimensions (groove width, pillar width and depth) depend on laser variables, such as laser power, scanning speed and number of passages, and drawing-based variables, as drawing pattern and dimensional features. Given these numerous variables, the selection of drawing features and laser parameters can be very demanding and time consuming. Therefore, research groups have dedicated effort towards optimization of surface textures, aiming different applications [32].

The goal of the present study was to explore the potential of the laser processing technique and analyse the influence of drawing and laser parameters to obtain a micro-scale pillars pattern which geometry and dimensions are suitable for the cellular ecosystem and, therefore, biomedical applications. In this context, this study explores the effect of laser and drawing parameters on the fabricated textures, by performing a design of experiments (DOE) and response surface method (RSM) to obtain a mathematical model for each texture dimension of interest. The final surfaces were evaluated regarding their geometry and dimensions,

roughness, wettability, and reproducibility.

2. Materials and methods

2.1. Laser surface texturing

Ti6Al4V alloy plates (ASTM B265), with chemical composition present in Table 1, were purchased from Titanium Products (United Kingdom) and cut into plates with dimensions of $9.0 \times 10.0 \times 0.5$ mm, using a Nd:YV04 laser (XM-30D, XianMing Laser, China) under an argon atmosphere.

Surface texturing was performed using a Nd:YAG laser (OEM Plus, SISMA, Italy), which specifications are summarized in Table 2.

A schematically representation of the laser processing is depicted in Supplementary Figure 1. Briefly, the laser power is controlled using a software interface and the laser beam is irradiated on the surface of the Ti6Al4V plate by a focusing unit containing fused quartz lens with a nominal focal length of 160 mm. The texture design (groups of vertical lines equally spaced and cross-hatched patterns for groove and pillars texturing, respectively) was defined in a computer-aided design software and then engraved on the metallic surfaces, according to specific laser parameters, through the laser connected Sisma Laser Controller (SLC) software. The texturing was assisted with a flow of air to remove sediments produced during laser processing. Afterwards, samples were cleaned in an ultrasonic bath with isopropyl alcohol (2-Propanol, Labsolve, Portugal) for 5 min and dried at room temperature.

The main goal of the present study was to explore micro-scale pillars texturing with pyramid elements with uniform size and spacing by laser surface texturing, with final dimensions in a selected range. For that purpose, the main steps were identified, as schematically illustrated in Fig. 1.

First, grooves were designed and textured to determine the groove width and depth. One to ten lines were engraved (Fig. 1A) by two different strategies: discrete laser processing and consecutive laser processing. In the former, the laser scans discrete zones at a time, creating one groove/laser ablation area and, afterwards the subsequent one, whereas in the second strategy the laser scans the total area of the sample consecutively (from left to right, and then returns to the beginning of the sample), as represented in Fig. 2.

Three laser scanning parameters were adjusted to optimize the texturing process: laser power, scanning velocity and number of passages. Laser power (P) corresponds to the laser beam energy delivered per pulse (Watts); the scanning speed (v) is the leading edge of the beam front speed (mm/s), and the number of passages (N) corresponds to the number of scans carried out by the laser during the process. Another parameter defined in the laser software is the line spacing (d), correspondent to the distance between the scanned lines in mm. These parameters were used to calculate, for each condition, the laser energy density in J/mm², by using Eq. (1):

$$E = \frac{P \, x \, N}{v \, x \, d} \tag{1}$$

In the grooves design and texturing step (Fig. 1A), the laser power was set at 3 or 6 W, the number of passages at 20, 40 or 80, the scanning speed at 50, 100, 200 and 400 mm/s and the line spacing at 10 μm, so that the laser energy density was either 120 or 240 J/mm². For each condition, the two scanning strategies were investigated. After evaluating the quality of the grooves, the consecutive laser processing was selected. Subsequently, two different marking approaches were studied: pre-set marking and continuous marking. In the former, the laser scans each line in one direction, whereas the latter marking mode employs a fill calculation method which connects parallel lines in a way that the laser remains on as much as possible, as shown in Fig. 3.

The continuous marking option presented a smoother surface compared to the one obtained by the pre-set marking and was, therefore, selected to investigate the combination of laser parameters and number

Table 1
Chemical composition of Ti6Al4V, according to manufacturer.

Material	Chemical composition (wt%, max)								
	N	C	H	Fe	O	Al	V	Ti	Other
Ti6Al4V	0.050	0.100	0.015	0.400	0.200	5.500–6.750	3.500–4.500	Matrix	0.500

Table 2
Laser Nd:YAG technical specifications.

Laser specifications	
Average output power (W)	6
Peak power per pulse (kW)	8.57
Wavelength (nm)	1064
Spot size (μm)	3
Pulse width (ns)	35
Repetition rate (kHz)	20
Maximum pulse energy (mJ/pulse)	0.3
Beam quality factor, $M^2 <$	1.8
Cooling system	Forced-air cooling

of lines considering the targeted distance between pillars. For texturing the micro-scale pillars (Fig. 1B), the laser power was set at 3 W, the scanning speed at 100 mm/s, the number of passages varied between 65 and 125 and the line spacing at 10 μm. Based on the selected laser power and features, processing was performed at a laser fluence of 12.6 J/cm^2, according to ISO 11146–2 [33]. Despite what was initially predicted, considering the same number of lines, the groove width obtained for the pillars texturing, i.e., distance between pillars, did not correspond to the groove width obtained for grooves texturing. Consequently, the number of lines was again adjusted to obtain the targeted groove widths, and the laser parameter combinations were again evaluated. Finally, the drawings were fine-tuned to obtain the targeted dimensions (Fig. 1C): groove width of 60±5, 90±5 and 120±5 μm, pillar width of 20±5 μm and pillar depth of 50±5 μm.

In a preliminary texturing of pillars by consecutive processing strategy, the horizontal lines were first engraved (from up to down)

followed by the vertical lines (from left to right), repeatedly by this order. It was observed that this strategy led to a variation of pillar depth along the sample. To counteract this effect and achieve a uniform pillar depth on the total sample area, the laser processing strategy was re-defined, still following the consecutive processing strategy. The horizontal lines were engraved from up to down followed by the vertical lines engraved from left to right and then the laser processing was performed in the opposite directions, i.e., horizontal lines were engraved from down to up and vertical lines from right to left. This laser processing order was repeated the selected number of passages.

2.2. Statistical analysis of the drawing and laser parameters

Response surface methodology (RSM) was used to analyse the relationship between explanatory variables (drawing and laser processing variables) and response variables (texture dimensions), which are depicted in Fig. 4.

Three predictive models were obtained, one for each texture dimension: groove width, pillar width and pillar depth. Each output response, R, is obtained through the construction of a polynomial mathematical relationship, correspondent to Eq. (2),

$$R = a_0 + \sum_{i=1}^{k} a_i x_i + \sum_{i=1}^{k} a_{ii} x_i^2 + \sum_{i<j}^{k} a_{ij} x_i x_j + \varepsilon \tag{2}$$

where a_0 is a constant, a_i is the linear coefficient, a_{ii} is the quadratic coefficient, a_{ij} is the interaction coefficient, x_i and x_j are the independent variables, k is the number of factors and ε is the associated error. These coefficients are predicted through regression analysis based on the measured responses.

(A) **Grooves design**
- Processing strategy: discrete vs consecutive
- Marking strategy: pre-set vs continuous
- 1-10 lines
- Evaluation of laser parameters

Measured features:
- Groove width
- Depth

(B) **Pillars design**
- Consecutive processing strategy
- Continuous marking
- 3, 6 and 9 lines
- Adjust laser parameters

Measured features:
- Pillar width
- Groove width
- Depth

(C) **Pillars design - Fine adjustment of drawing and laser parameters**
- Consecutive processing strategy
- Continuous marking
- 6, 9 and 12 lines
- Adjust laser parameters

Measured features:
- Pillar width
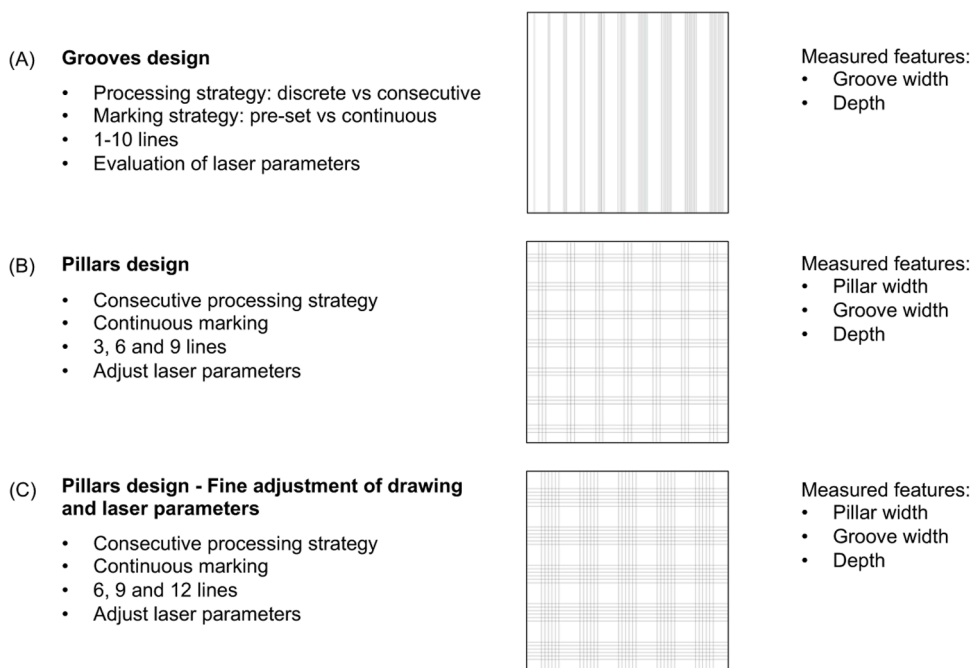- Groove width
- Depth

Fig. 1. The study of the micro-pillar surface laser texturing was divided into three main steps: (A) grooves design and texturing, followed by (B) pillars design and texturing and, finally, (C) a fine adjustment of the drawing and laser parameters to obtain a micro-scale pillars pattern with uniform size and dimensions in the selected range.
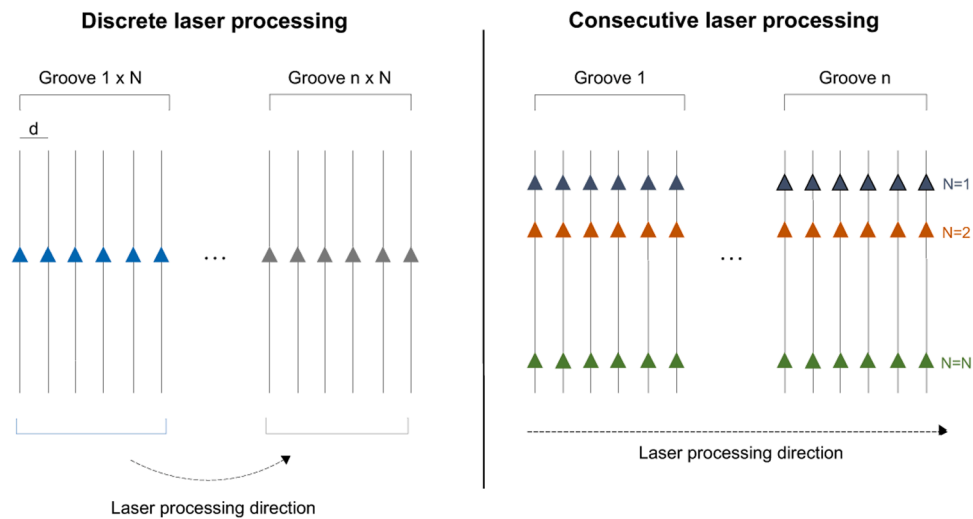
Fig. 2. Schematic representation of the grooves texturing processing, in which n is the number of grooves engraved by scanning vertical lines, spaced in between by d, in discrete and consecutive processing strategies. In the former, the laser engraves each groove (represented by one colour) at a time, whereas in the latter strategy each line is engraved consecutively from left to right, N number of passages (each passage is represented by one colour).
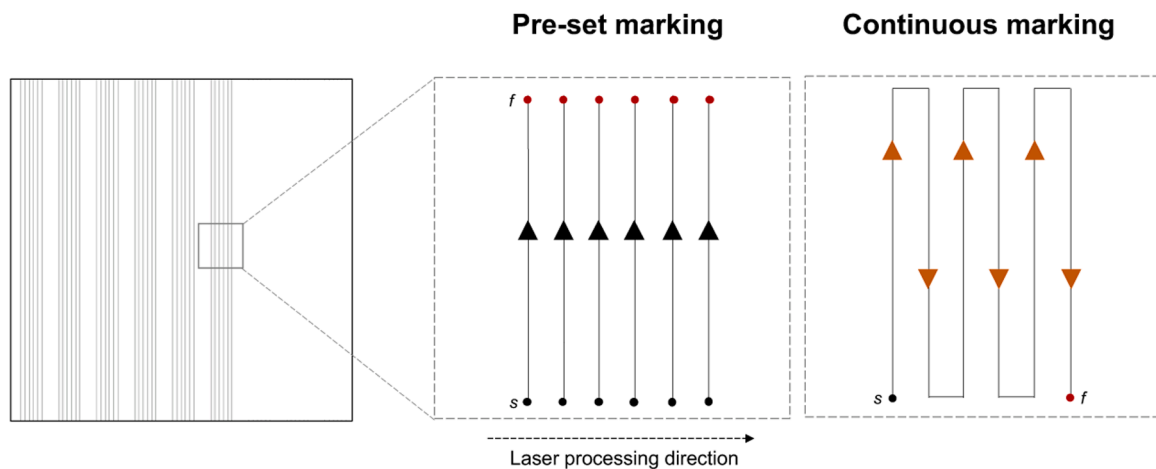

Fig. 3. The laser surface texturing begins at the point s (starting point) and finishes at f (finishing point), considering the laser scanning from left to right. In the pre-setmarking approach the laser direction is from down to top repeatedly, whereas in the continuous marking parallel lines are connected so that the laser remains on as much as possible.
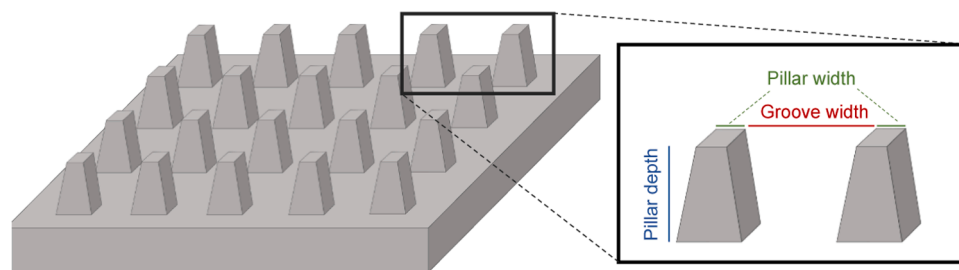

Fig. 4. Representation of the pillar laser texture dimensions: groove width, pillar width and pillar depth.

Table 3
Multilevel factorial design of the experiment, including the input parameters and corresponding levels.

Input parameters		Input levels								
A_CAD	Groove width (μm)	3-level	50			80			110		
B_CAD	Pillar width (μm)	3-level	30			35			40		
N	Number of passages	9-level	65	70	75	80	85	110	115	120	125

The experimental matrix considering the levels of each parameter, summarized in Table 3, was constructed using Minitab software, which included a total of 81 combinations, as presented in Supplementary Table 1.

The obtained texture dimensions were measured as described in Section 2.3.1. and the experimental data was inserted in the Minitab software. Using the RSM tool, the results were analysed, and the three mathematical models obtained. Afterwards, ANOVA was applied to each mathematical model with a 95% confidence interval to investigate the reliability, namely the contribution of each individual and combined parameters in the final response.

2.3. Surface characterization

2.3.1. Surface topography

Textured samples were analysed by scanning electron microscopy (SEM) using JSM-6010 LV (JEOL, Japan). The surface of groove textured samples was assessed by SEM and texture dimensions were calculated using the ImageJ software. The groove width was measured by averaging five measures using a top view SEM image and the groove depth using a cross-section SEM image view.

The topography of pillar textured samples was assessed by a S neox 3D Optical Profiler (Sensofar, Spain) with a 10X objective and analysed with the Gwyddion software to assess the texture dimensions. The 2D profile was acquired in the horizontal direction and each texture dimension corresponded to the average of five measurements. For a better comprehension, texture dimensions were grouped according to the study timeline: first, the goal setting dimensions were selected, then the drawing dimensions were defined in a CAD file and finally, after processing, the dimensions were measured by profilometry. As opposed to the groove width and pillar width, which are strongly influenced by the 2D drawing dimensions (A_CAD and B_CAD), the desired pillar depth is primarily achieved by selecting the appropriate laser parameters, particularly the number of passages (N). The abbreviation of each dimension denomination is summarized in Table 4.

2.3.2. Surface wettability

The wetting behaviour of post-processed samples was assessed using the contact angle system OCA 15 plus (Dataphysics, Germany). Samples were ultrasonically cleaned with isopropyl alcohol for 5 min, stored at 60 °C overnight and stored in a desiccator. 180 days after surface laser texturing, a 4 µL droplet of distilled water was dispersed at a dosing rate of 1 µL/s at room temperature and the contact angles were determined using the DataPhysics SCA software.

2.3.3. Surface roughness and shape factor

Sample roughness can be obtained at a micro or macro scale. In the former, Ra and Rq were obtained by averaging ten measurements by selecting 2D profiles both in horizontal and vertical directions. At a macro-level, within a defined sample area, Sa, Sq and Sku of the 3D surface texture were obtained. The latter was used to evaluate the sharpness of the surface height distribution, which may be skewed above the mean plane (Sku<3), normal and thus sharp when indented portions co-exist (Sku=3) or spiked (Sku>3), as illustrated in Fig. 5 [34]. The roughness values were obtained for an area of interest defined in the Gwyddion software.

To quantitively evaluate the shape of the textured pillars, a formula to determine the geometry shape factor was defined in Eq. (3). The

Table 4
Texture dimension denomination along the study.

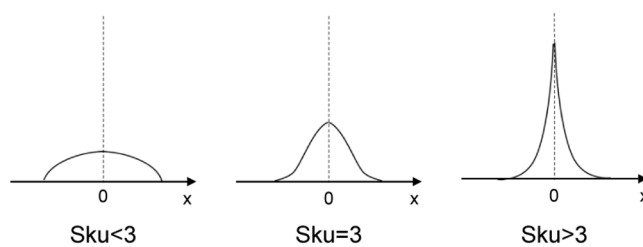|	Goal (G)	2D Drawing (CAD)	After processing (AP)
Groove width (A)	A_G	A_CAD	A_AP
Pillar width (B)	B_G	B_CAD	B_AP
Pillar depth (C)	C_G	–	C_AP

Fig. 5. Sku measures the sharpness of the roughness profile.

shape factor was calculated for the input variables combinations which texture dimensions, after processing (AP), were closer to the range of the targeted dimensions.

$$Shape\ factor = \frac{D}{d} \qquad (3)$$

in which D is the groove width and d the distance correspondent to the horizontal plane of the groove, as represented in Fig. 6.

3. Results and discussion

The main goal of the present study was to explore the capability for obtaining a micro-scale pyramid pillars pattern by laser surface texturing with groove width (A_G) of 60±5, 90±5 and 120±5 µm, pillar width (B_G) of 20±5 µm and pillar depth (C_G) of 50±5 µm. The study was focused, first, on the design and texture of grooves with the targeted widths and then on adjusting the laser and drawing parameters to design and texture pillars with uniform size and equally spaced with dimensions in the defined range.

3.1. Grooves design and texturing

3.1.1. Discrete vs consecutive processing laser

In this study, two laser scanning strategies were evaluated: discrete and consecutive laser processing, which principle is shown in Fig. 2. Considering the same laser parameters, and thus the same laser energy density, the consecutive laser processing strategy resulted in smoother grooves, as presented in Fig. 7. When scanning the overall sample through consecutive laser processing, the generated temperature in the groove is lower compared to when creating discrete grooves, leading to a lower number of defects and thus smoother grooves [35].

3.1.2. Pre-set vs continuous marking

Besides the machining strategy, two laser marking approaches were investigated: pre-set and continuous marking, as schematically represented in Fig. 3. The latter was selected due to the obtained smoother surface, as shown in Fig. 7.

In the pre-set marking, the laser goes on/off on each line which may, therefore, present some power variations. On the contrary, in the continuous marking mode, the laser is as close as possible to be always on throughout the whole processing process, and thus, the laser power distribution is more uniform and constant. Nevertheless, the grooves-textured surfaces present some debris, which are typical for a LST process [36]. Different laser parameters were evaluated for both laser processing and marking strategies and the obtained groove width and depth of one to ten lines engravement are summarized in Supplementary Tables 2 and 3. The laser power was set at 3 or 6 W, the scanning speed at 50, 100, 200 and 400 mm/s and the number of passages at 20, 40 or 80 so that the laser energy density was either 120 or 240 J/mm^2.

The first main step included the design and texture of grooves to evaluate the effect of some drawing and laser parameters on the obtained groove width and depth. Discrete and consecutive laser processing strategies were investigated, and a smoother surface was achieved on the consecutive laser processing. Afterwards, the pre-set
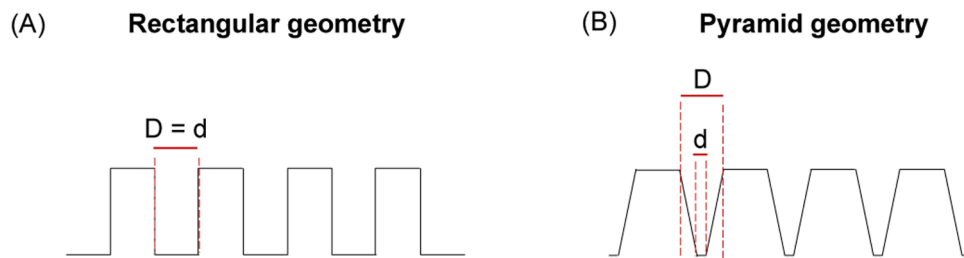
Fig. 6. The shape factor of a (A) rectangular geometry is equal to one, whereas a (B) pyramid geometry presents a shape factor higher than 1 (*D>d*).
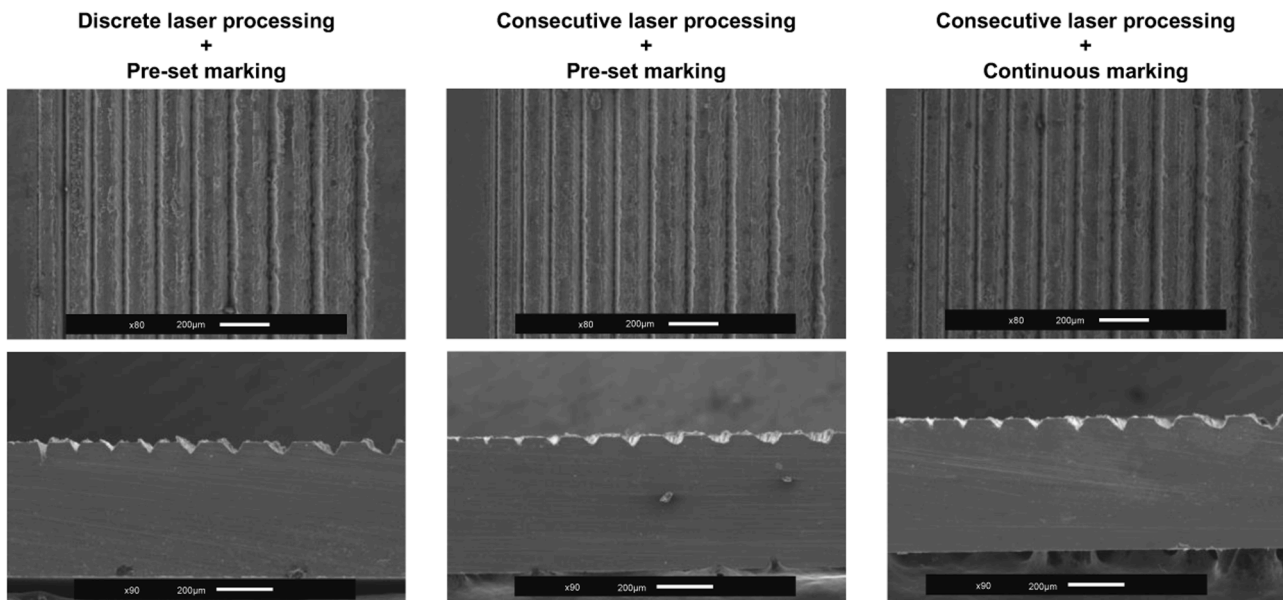

Fig. 7. Top and cross-section scanning images of discrete laser processing (left) and consecutive laser processing (middle) strategies by pre-set marking and consecutive laser processing and continuous marking (right). One to ten lines (from left to right) were engraved with 3 W laser power, scanning speed of 100 mm/s and 80 laser passages.

and continuous marking modes were compared, and the latter was selected for this study. A more uniform laser energy distribution for the continuous marking mode resulted in a surface with less debris and smoother ablated zones.

3.2. Pillars design and texturing

After selecting the consecutive laser processing as the machining strategy and the continuous marking mode, the obtained groove width and depth were evaluated to select the laser power, scanning speed and number of lines for pillars design and texturing. The laser power was set at 3 W, the scanning speed at 100 mm/s and the CAD drawings of cross-hatched patterns were designed with groups of 3, 6 and 9 lines, as shown in Fig. 1B. However, the groove width obtained by processing grooves (groups of vertical lines) was higher than the groove width obtained for the cross-hatched pattern (groups of vertical and horizontal lines), considering the same number of lines and laser parameters. This is probably related to the fact that texturing grooves is faster, because only vertical lines are engraved (from left to right). Consequently, the temperature of the textured sample is higher when the laser returns to the beginning and the accumulated heat in the ablation area leads to a wider machined area [35,37]. For this reason, the number of lines was adjusted to 6, 9 and 12 lines to obtain the targeted groove widths (60, 90 and 120 µm, respectively), as schematically represented in Fig. 8A-C. Besides the number of lines, which is predicted to directly influence the groove width, another drawing parameter is the distance between the groups of lines, which was set as 30, 35 and 40 µm, as shown in Fig. 8D-F.

The laser parameters were fixed to a power of 3 W, the scanning speed to 100 mm/s and the number of passages was varied between 65 and 125, making a total of 81 combinations, as summarized in Supplementary Table 1.

When texturing the cross-hatched design pattern, the laser ablation is increased when the vertical and horizontal lines are intersected. In fact, on those areas, the number of passages is the double, creating high depth holes as demonstrated in Fig. 9.

3.3. Mathematical models

For each experiment the texture dimensions (A_AP, B_AP and C_AP) were measured and collected to perform a statistical analysis. A two-second order regression model was developed for each texture dimension and the effect of individual and combined variables were investigated using ANOVA. The coefficients reflect the main effects of the drawing and laser processing parameters and their interaction. The relationship between the responses and single input variables is statistically significant for all models ($p < 0.001$). Furthermore, the interaction between variables has a significant effect, proving that LST is a complex process and that the texture dimensions are a result of the interaction of multiple variables. In this sense, mathematical models are a crucial tool to understand the effect of drawing and laser processing input variables, and to predict the texture dimensions for a particular set of input variables. All models are normally distributed and present hetero-scedasticity, as shown by the plot of regular residuals and residuals
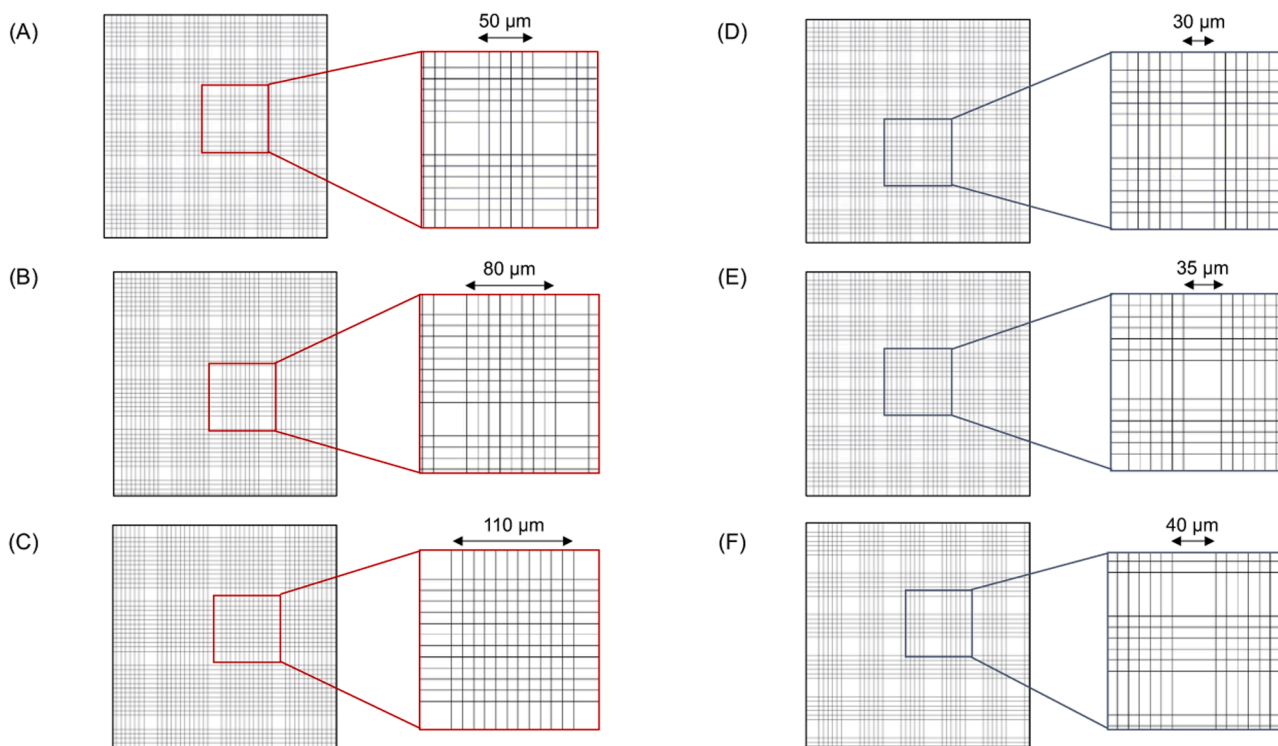
Fig. 8. CAD drawings of cross-hatched patterns with a groove width of (A) 50 μm, (B) 80 μm and (C) 110 μm and pillar width of (D) 30 μm, (E) 35 μm and (F) 40 μm, in this case exemplified for the design pattern with a groove width of 50 μm.
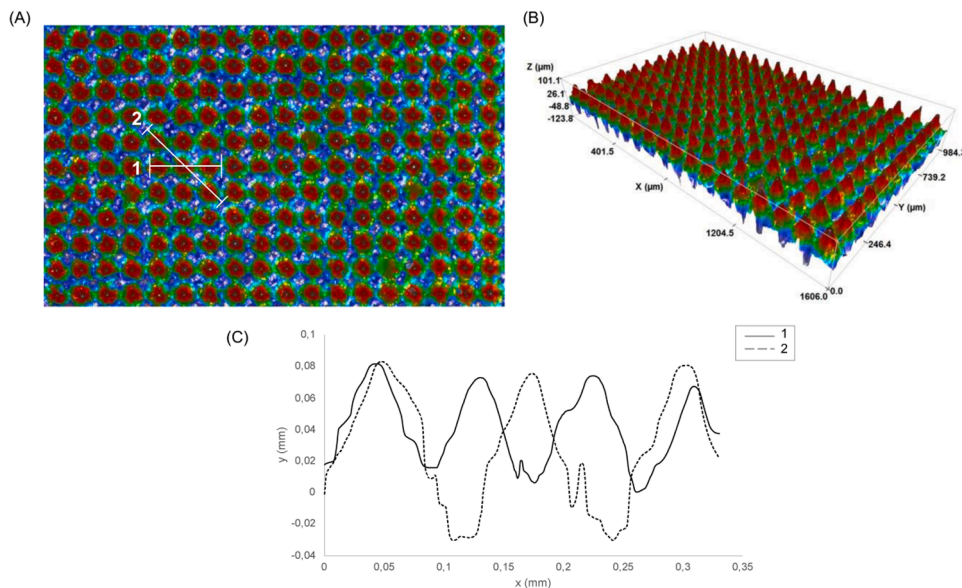

Fig. 9. (A) 2D and (B) 3D optical profilometry images of a textured sample and the corresponding (C) extracted profiles, in which the black corresponds to the horizontal line and the grey to the diagonal one. Pillar peaks are in red and deeper holes in blue. The displayed images were acquired for Exp. No. 35 (A_CAD = 50 μm, B_CAD = 40 μm and N = 70). (For interpretation of the references to colour in this figure legend, the reader is referred to the web version of this article.).

versus fitted values in Supplementary Figures 2–4.

One model for each texture dimension of interest (groove width, pillar width and depth) was proposed, as follows.

a) **Groove width model**

The mathematical model of the groove width, simplified with only significant terms, is described in Eq. (4).

$$Groove\ width\ (\mu m) = -13.1 + 1.475A + 1.16B - 0.501N - 0.002666A^2 - 0.01001BN$$

(4)

The suitability of the developed groove width model and the significance of linear and second order terms and the two-way interactions between terms are presented in Supplementary Table 4. The P-values of A, B and N are lower than 0.05, indicating that these factors are

extremely significant for the groove width regression model. The interactions A^2 and BN are also significant terms (*p*-value<0.05). The groove width model describes the response given a low value of S (S = 1.91) and the regression is approximately 100 (R^2 = 99.40%), which indicates that 99.40% of the groove width variation can be explained by the regression model and thus the data fits the model. In addition, the high values of adjusted R^2 and predicted R^2 suggest that the model is adequate for the prediction of the groove width values within a confidence interval of 95%. In addition, the high F-value of the model (1311.78) indicates that the proposed model is significant.

a) **Pillar width model**

The pillar width mathematical model is described in Eq. (5), simplified with only significant coefficient, and the suitability of the model and significance of the terms are presented in Supplementary Table 5.

$$Pillar\ width\ (\mu m) = 17 - 0.284A - 1.03B + 0.540N + 0.001236A^2$$
$$- 0.00747BN \qquad (5)$$

The P-values of A, B and N are extremely significant due to their P-value lower than 0.05. Regarding the interactions, A^2 and BN are the only significant interactions (P-value< 0.05). Although the S value is still considered low (S = 2.02), only 61.01% of the variation can be explained by the regression model. The adjusted R^2 and predicted R^2 values are close to 61%, suggesting that the model can only be used for a short acting range. In fact, the B_CAD was only varied between 30 and 40, which is suggested to be the main reason for a not high F-value (12.34). Nevertheless, the residual plots fall on a linear trend and the obtained model can be used for the pillar width range that was defined as target in this study.

a) **Pillar depth model**

The third mathematical model is the pillar depth model, which is plotted in Eq. (6), reduced to only significant coefficients. The suitability

and the significance of linear and second-order terms are presented in Supplementary Table 6.

$$Pillar\ depth\ (\mu m) = -297.8 - 1.447A + 19.29B - 1.627N - 0.00492A^2$$
$$- 0.3243B^2 + 0.00685AN + 0.06558BN + 0.06480AB$$
$$(6)$$

All linear terms (A, B and N) and the interactions A^2, B^2, AN, BN and AB have a P-value lower than 0.05, which means they are significant terms for this model. Although the S of the depth model is higher than 2 (S = 5.97), the model is still acceptable given the regression close to 100 (R^2 = 98.02%), as well as the high values of adjusted R^2 and predicted R^2, which suggest a proper fitting. Furthermore, the high F-value of the model (391.43) implies that the depth model is significant. In this sense, the proposed model for pillar depth is adequate for predicting depth values with a confidence interval of 95%.

3.3.1. Effect of the parameters on texture dimensions

The statistical analysis performed on the three mathematical models suggests that groove width (A_CAD), pillar width (B_CAD) and number of passages (N) have a significant effect on the texture dimensions (P-value<0.05). The main effects of each parameter on groove width (A_AP), pillar width (B_AP) and depth (C_AP) are plotted in Fig. 10.

As initially predicted, the A_CAD has a proportional and evident effect on the groove width after processing. Although not so pronounced, a higher B_CAD increases the groove width, on contrary to the number of passages which does not have a linear effect (Fig. 10A). The pillar width increases, not linearly, with N and A_CAD and decreases with increasing B_CAD (Fig. 10B). Close to a linear tendency, the pillar depth increases with A_CAD, B_CAD and N.

Sen et al. studied the influence of laser processing parameters on micro-groove texturing of Ti6Al4V substrates using a fibre laser. The increment of the number of passages resulted in an increase of groove depth and width, the latter up to a certain number of passages because of the re-solidification of the molten material [38]. The correlation between picosecond laser processing parameters and the corresponding micro-groove dimensions were also assessed and the authors concluded
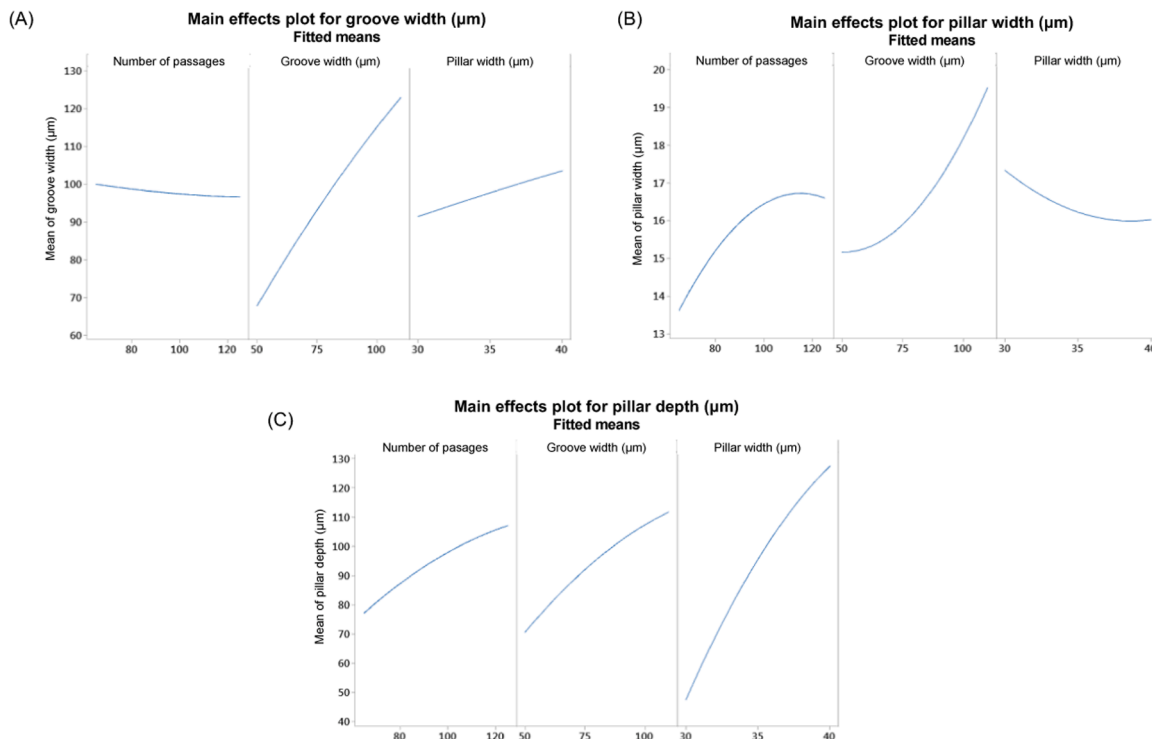

Fig. 10. Main effects of each parameter on (A) groove width, (B) pillar width and (C) pillar depth.

that increased groove depth was obtained by increasing the number of passages or decreasing the scan speed [39]. According to Eq. (1), higher number of passages reflects a higher laser energy density, considering the same laser power, scanning speed and line spacing defined in the laser processing. In this sense, high laser energies result in higher pillar depths as a consequence of the greater ablation [40]. The same conclusion was claimed by Soveja et al., in which the analysis of developed mathematical models showed that the pulse energy was the most influential factor on the material removal rate [32].

Besides the significant contribution of each linear term, according to the analysis of variance present in Supplementary Tables 4–6, the combination of both pillar width (B_CAD) and number of passages (N) have a significant effect ($p<0.005$) on the groove width (A) and pillar width (B), whereas the combinations of the three variables have a significant effect ($p<0.005$) on the pillar depth (C). To better understand the effect of the second-order interactions in each texturing response, contour plots of the developed mathematical models are present in Fig. 11.

The contour plots confirm that each texture dimension is well described by the developed mathematical models. The significant interactions of the input parameters on the three mathematical models are summarized in Table 5.

For the groove width model and focusing on the target groove widths (A_G = 60±5, 90±5 and 120±5 μm) the interactions A_CAD vs B_CAD and A_CAD vs N are not significant. On the other hand, the interaction between B_CAD and N has a significant effect on the groove width (e.g., comparison between Exp. No. 62 and 33). Considering the actuation range predicted by the pillar width model, the interaction between B_CAD and N has a significant effect (e.g., by comparing Exp. No. 54 and 57). On the contrary, for the target pillar width (B_G = 20±5 μm) the interactions A_CAD vs B_CAD and A_CAD vs N do not have a significant

Table 5

Significant effect of combined parameters in the final response for the obtained mathematical models.

Model	Exp. No.	A_CAD (μm)	B_CAD (μm)	N	Output texture dimension (μm)	Significant interaction
Groove width model	62	80	30	70	A_AP = 97.6	B_CAD vs N
	33			125	A_AP = 90.4	
Pillar width model	54	80	30	75	B_AP = 15.4	B_CAD vs N
	57			115	B_AP = 21.6	
Pillar depth model	49	80	30	85	C_AP = 37.5	A_CAD vs B_CAD
	63	110			C_AP = 59.5	
	57	80	30	115	C_AP = 47.2	B_CAD vs N
	52		40		C_AP = 144.1	
	60	50	35	65	C_AP = 54.2	A_CAD vs N
	42			120	C_AP = 73.9	

effect. The only mathematical model which is strongly dependent on all input variables combinations is the pillar depth model. By focusing on the target pillar depth (C_G = 50±5 μm), the following combinations have a significant effect: A_CAD vs B_CAD (e.g., comparison between Exp. No. 49 and 63), B_CAD vs N (e.g., comparison between Exp. No. 57 and 52) and finally A_CAD vs N (e.g., comparison between Exp. No. 60 and 42).

The proposed mathematical models are therefore suitable to predict the texture dimensions for a set of input drawing and laser processing variables, for the range of dimensions selected for this study.
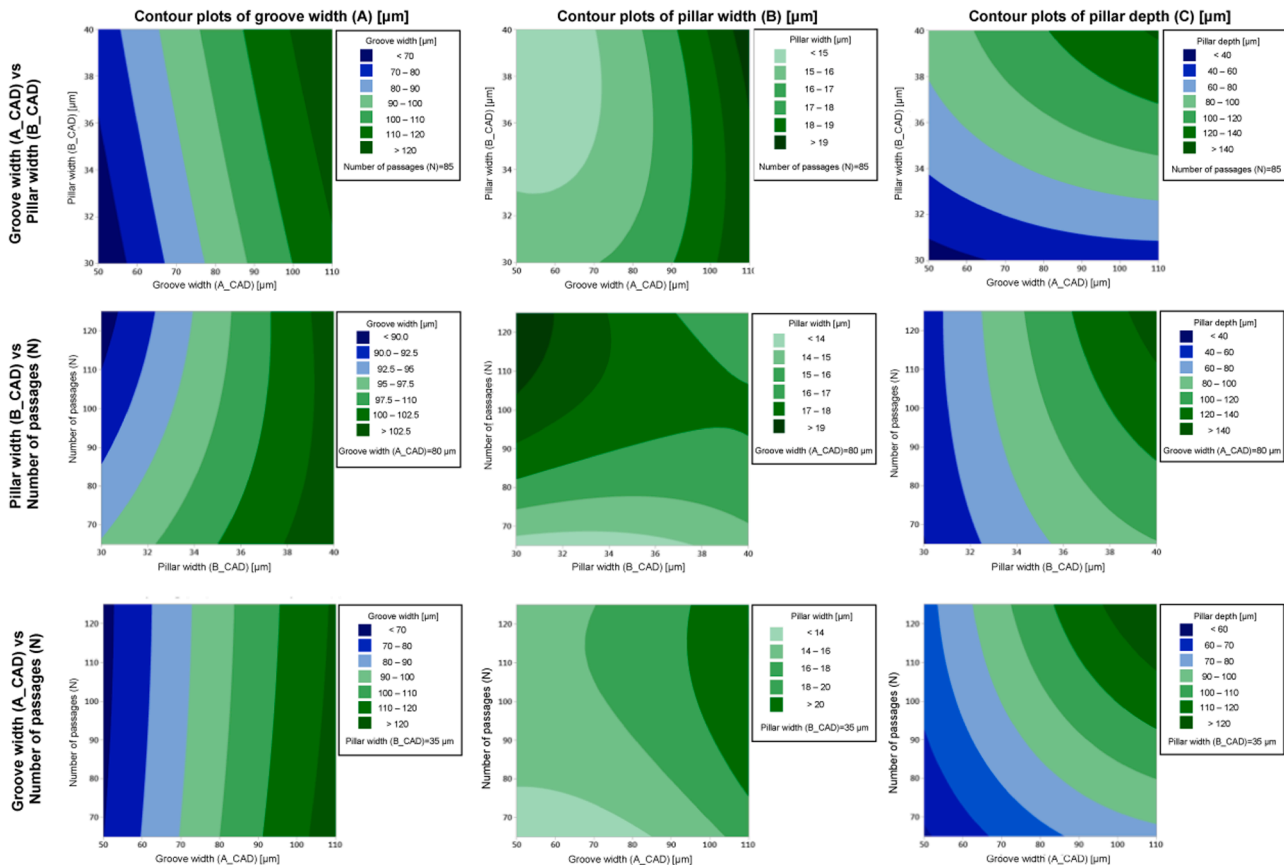

Fig. 11. Contour plots of groove width (A), pillar width (B) and pillar depth (C) in response of the combination of the input variables (A_CAD, B_CAD and N), by holding the third variable at the middle of its range.

3.4. Characterization of textured samples

Topology and morphology of metallic surfaces can be modified by laser processing and achieved by changing the laser parameters. In fact, micro-scale patterns with pyramid elements were successfully obtained, with different texture dimensions. Considering each target texture dimensions, three combinations of drawing and laser processing parameters were selected, as displayed in Table 6.

As any machining process, laser texturing presents a tolerance due to, for example, laser positioning and inherent error of the technology. Nevertheless, there is flexibility to adjust the drawing and laser parameters to obtain a micro-scale pillar pattern with dimensions of interest.

3.4.1. Wettability

The wetting behaviour of textures which dimensions are in the range of the target was assessed by sessile drop measurement with distilled water and is displayed in Fig. 12. Surfaces with water contact angles (WCA) under 90° are defined as hydrophilic and above 90° as hydrophobic [41].

When considering smooth surfaces, wetting is assessed by the Young model. However, two theories have been proposed to characterize the wetting behaviour on micro-structure surfaces: Wenzel and Cassie-Baxter solid-liquid wetting states. On the former, the water droplet penetrates the grooves, whereas on the latter the water droplet is suspended on the top of the texture features [42]. Given the heterogeneity associated to laser processing, textured samples are not smooth and thus air may be entrapped in surface irregularities, increasing the contact angle [43]. In addition, variations between the real and ideal surface contribute to contact angle hysteresis which influences the contact angle measurement [44]. Wettability of a solid surface is, therefore, determined by the surface morphology and topography, but also by its chemical composition [45]. Despite the fact it is a muti-variable dependent feature, some authors investigated the correlation between laser textured surfaces and wetting. Wang et al. performed pulsed laser ablation in liquid to engrave a grid pattern (spacing between adjacent scanning lines of 150 μm) on Ti6Al4V by nanosecond laser pulses [46]. The raw Ti6Al4V surface presented a contact angle of 77° and after texturization in air, deionized water and ethanol it increased to more than 150°. The transition to hydrophobic state was hypothesized to be
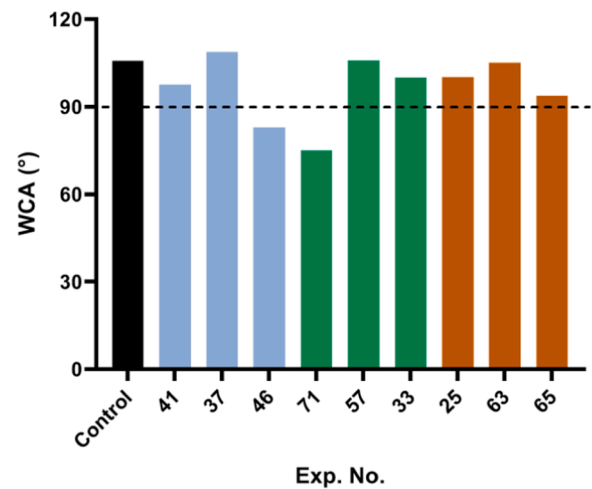

Fig. 12. Water contact angles of the experiment numbers which dimensions after processing are in the range of the target texture dimensions. The dark bar corresponds to the control group (non-textured), blue bars to textures with A_G = 60±5 μm, green bars to A_G = 90±5 μm and orange bars to A_G = 120±5 μm. The demarcation of hydrophilic and hydrophobic behaviour is represented by a dashed line at 90°. (For interpretation of the references to colour in this figure legend, the reader is referred to the web version of this article.).

related to the weak adhesion between textured surfaces and the droplet, impairing the complete immersion of the droplet (Cassie-Baxter state) and to the absorption of organic species during laser ablation which changed the surface polarization and thus the surface wettability [46]. In addition, storage conditions, in which are included the period of time between texturing and the contact angle measurement, have been shown to influence wetting. Raimbault et al. fabricated grooves on Ti6Al4V by a femtosecond Yb-YAG laser (groove width of 25, 50 and 75 μm and depth of 1 or 5 μm) and concluded that contact angles increased in the days following the irradiation due to the passive hydrophobic hydrocarbon layer amplified by the surface topography [47]. Patel et al. observed that pillars textured samples presented a wetting behaviour up to 24 h after Nd:YAG laser irradiation but was altered to hydrophobic over time [23]. Similar behaviour was found by the study conducted by Yang et al., in which a nanosecond pulser laser was used to create line, grid and spot patterns on Ti grade 2. Immediately after laser treatment, surfaces were more hydrophilic while, after long-term exposure to air, the contact angles increased to more than 130° [45].

Compared to the non-textured group, textured surfaces displayed similar or lower contact angles. Laser treatments alter surface features, such as surface structure, roughness and chemical composition, and the combination of these dictate the surface wettability. Hydrophilic surfaces improve the interaction between the biomaterial and the in vivo environment and thus, adding textures to titanium samples by LST can increase their wettability, contributing to better osseointegration outcomes.

3.4.2. Roughness, topography and morphology

The roughness of each texture may be acquired either by 2D profiles or by selecting a specific surface area. Amplitude parameters are considered the most important parameters to characterize the surface topography, as they are used to measure the vertical characteristics of surface deviations. Ra and Rq were calculated at the horizontal plane of grooves and Sa, Sq and Sku considering the surface of interest, as summarized in Table 7. Other parameters related to the surface roughness are shown in Supplementary Table 7.

A pyramid geometry was obtained through laser processing, as illustrated in Fig. 13, due to the Gaussian beam energy distribution. In order to quantitively assess the pillars geometry, a shape factor was calculated according to Eq. (3). The shape factor was calculated for the

Table 6

Combinations of drawing and laser parameters for the targeted dimensions (groove width (A_G) of 60±5, 90±5 and 120±5 μm, pillar width (B_G) of 20±5 μm and pillar depth (C_G) of 50±5 μm).

Exp. No.	Input parameters			Output texture dimensions			
	A_CAD (μm)	B_CAD (μm)	N	Groove width		Pillar width B_AP (μm)	Pillar depth C_AP (μm)
				A_G (μm)	A_AP (μm)		
41	50	40	75	60±5	70.5± 2.7	16.2 ± 1.5	78.8 ± 4.0
37		30	125		60.2 ± 2.8	16.6 ± 3.4	33.9 ± 3.2
46		30	80		60.0 ± 3.8	18.3 ± 1.2	32.4 ± 6.5
71	80	30	80	90±5	91.4 ± 3.0	19.0 ± 2.8	44.1 ± 2.9
57		30	115		88.2 ± 4.0	21.6 ± 4.0	47.2 ± 3.9
33		30	125		90.4 ± 2.4	18.6 ± 2.6	47.9 ± 5.2
25	110	30	70	120 ±5	121.6 ± 4.4	15.4 ± 2.8	50.7 ± 4.1
63		30	85		120.8 ± 3.5	19.2 ± 2.8	59.5 ± 3.5
65		30	125		114.2 ± 1.6	20.8 ± 4.2	54.0 ± 2.6

Table 7

Groove and surface roughness values and shape factor of the experiment numbers which dimensions after processing met the target texture dimensions.

Exp. No.	Ra (µm)	Rq (µm)	Sa (µm)	Sq (µm)	Sku	Shape factor
41	2.73 ±1.72	3.08 ±1.93	32.21	39.91	−0,32	3.94±0.65
37	1.66 ±0,83	2.12 ±1.12	13.89	17.68	0,35	4.46±0.92
46	1.68 ±0.59	2.01 ±0.76	13.74	17.99	0,85	4.83±0.62
71	2.17 ±1.10	2.68 ±1.35	24.22	31.07	0,31	3.76±0.83
57	2.23 ±1.10	2.70 ±1.28	25.18	32.02	0,25	5.02±0.85
33	1.88 ±0.63	2.26 ±0.81	24.1	31.23	0,51	4.19±0.52
25	2.36 ±0.97	2.70 ±1.09	31.22	38.75	−0,29	2.32±0.21
63	2.43 ±1.23	3.04 ±1.50	30.27	37.89	−0,15	2.54±0.37
65	1.96 ±1.24	2.40 ±1.47	29.78	38.21	0.25	3.11±0.44

selected combinations through the 2D profilometry profile, as exemplified in Fig. 6. The rectangular shape was adopted as the comparing element and the calculated shape factors are summarized in Table 7.

When in direct contact with bone, the surface properties of metallic implants must elicit a cellular response that promotes bone regeneration and assures an implantation success. The mechanisms underlying the interaction between cells and biomaterials are complex and the optimal surface topography responsible for eliciting the target application remains a critical challenge. Surface treatment by a nanosecond laser is a promising technique to create specific topographies. In the current study, micro-pillar patterns with pyramid elements and different texture dimensions were textured on Ti6Al4V samples.

Chikarakara et al. performed a high-speed CO_2 laser melting of Ti6Al4V which resulted in a modified layer from 20 to 50 µm deep with improved microstructural properties [48]. Afterwards, the improved biocompatibility of these laser-treated surfaces (with average roughness values between 1.39 and 2.73 µm) was demonstrated by culturing fibroblast and osteoblast cell lines [49]. Topological features, such as micro-grooves, have been shown to regulate contact guidance which influences cell adhesion, shape and orientation and therefore the cellular response. Mukherjee et al. used a long-pulsed laser to create micro-ripple topographies on Ti6Al4V surfaces with different sizes (20, 40 and 100 µm width). Human MSC were prominently orientated on surfaces having 20 µm ripples (3D average roughness of 1.9 µm) and showed the highest differentiation potential towards osteoblastic

lineage [50]. Voisey et al. textured groove arrays (40 µm width, 10 µm depth and ridge width of 20 µm) on commercially pure titanium using a Q-switched laser and the obtained surface with a Sa of 18±03 µm and groove Ra of 0.8±0.01 µm promoted a preferential alignment of human osteosarcoma cells with the groove length [51]. Zheng et al. machined micro-grooves on Ti6Al4V surface by a fibre laser marking machine (depth 10 µm, width 10, 20 and 30 µm and pitch 60, 105 and 150 µm) and higher roughness values (2.72±0.52 µm) improved MC3T3-E1 cell adhesion and biological activity [52]. Micro-texturing increases the surface area and rougher and hydrophilic or near hydrophilic surfaces promote adhesion, spreading and proliferation of cells and thus its potential application in bone tissue engineering. Laser texturing was performed in other materials which also promoted a positive cellular response. In vitro studies were conducted on squared ridges of ~50 × 50 µm² (grooves with 100 µm width 80 µm depth) textured on a zirconia substrate using a Nd:YAG laser. The surface with Ra<3 µm, Sa of 17.1 µm and Sq of 21.4 µm promoted the attachment and proliferation of MC3T3-E1 cells [53].

The obtained surface roughness values are in line with the literature for laser texturing on metallic materials. Furthermore, surface roughness between 20 nm and 10 µm were reported to have a positive impact on the biocompatibility of metallic materials, as cells and biological molecules have an approximate length scale [54]. In the present study, the textured pillars have a pyramid shape (shape factor>1), and surface laser texturing may be used to create a micro-scale design with uniform size pillars that are evenly spaced. A set of drawing and laser parameters were selected for each targeted pattern dimensions as follows: A_CAD = 50, 80 µm and 110, B_CAD = 30 µm and N = 80 (for A_CAD = 50 and 80 µm) and N = 125 (for A_CAD = 110 µm), which correspond to a laser energy density of 240 and 375 J/mm² (for 80 and 125 laser passages, respectively). The selected samples were hydrophilic or near hydrophilic and the roughness parameters and shape factors are similar for the three selected combinations. The micro-scale pillars texture of each selected sample was assessed by SEM, as represented in Fig. 14.

4. Conclusions

The search for an improved surface micro-geometry on metallic implants, able to efficiently promote bone regeneration, remains a challenge. Laser surface texturing has been proposed as a promising tool to modify the surface of metallic biomaterials. However, several parameters including drawing and laser processing parameters, such as laser power, scanning velocity and number of passages, significantly influence the surface geometry and properties. The present study aimed to explore the capabilities of laser surface texturing on Ti6Al4V samples and, by assessing the influence of drawing and laser parameters, a set of input parameters was selected to obtain a micro-scale pattern with
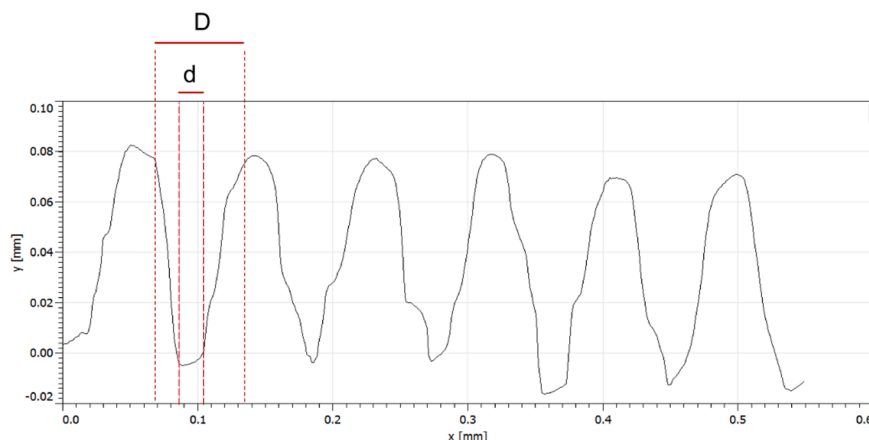

Fig. 13. The shape factor was calculated by randomly selecting lines in the 2D profile, as the acquired for Exp. No. 41 (A_CAD = 50 µm, B_CAD = 40 µm and N = 75).
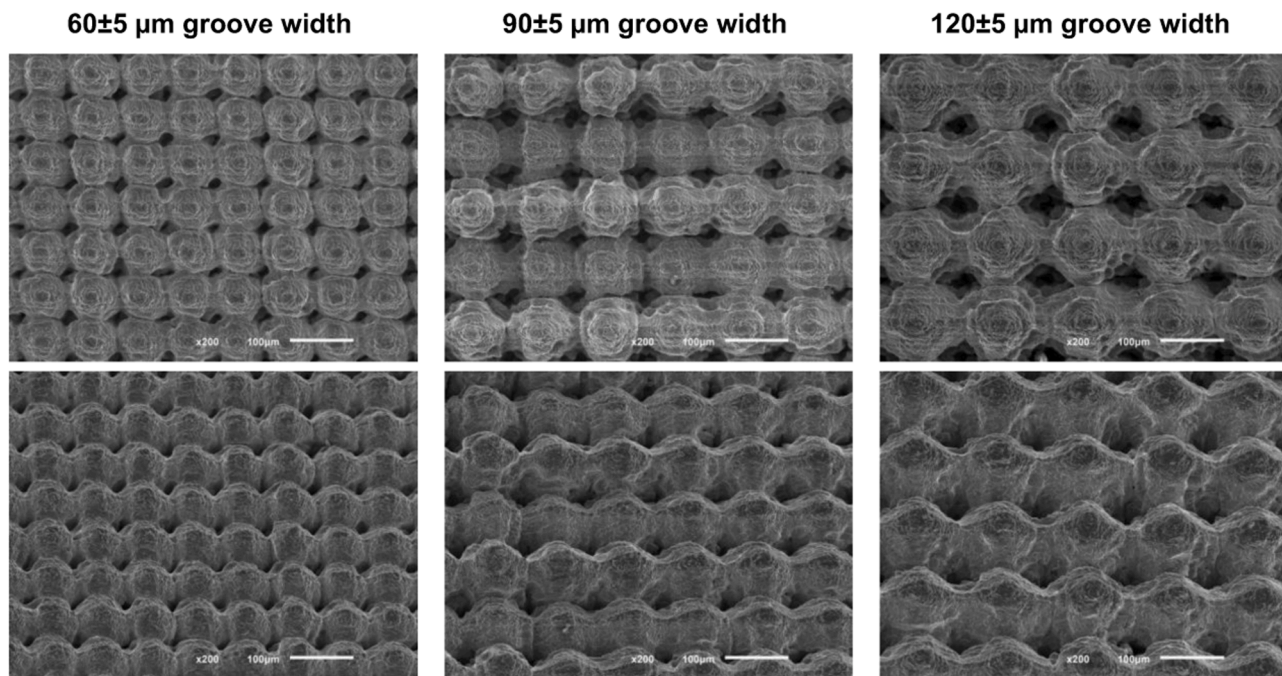
60±5 μm groove width   90±5 μm groove width   120±5 μm groove width

Fig. 14. SEM images of the selected patterns (top view and with tilting of 30°). The micro-scale pattern with pillar width of 20±5 μm, depth of 50±5 μm and groove width of 60±5, 90±5 and 120±5 μm correspond to the Exp. No. 46, 71 and 65, respectively.

pyramid pillars with dimensions targeted for biomedical applications. On grooves texturing, two laser machining strategies and marking modes were investigated. The consecutive laser processing strategy and continuous marking mode were selected given the smoother grooves. Afterwards, a pillar pattern was designed and textured within a set of input drawing and laser parameters. Predictive models were developed for each texture dimension (groove width, pillar width and depth) and the main contributions of the input parameters were correlated with each dimension. This processing strategy was effective to obtain micro-scale patterns and input combinations were selected based on the targeted dimensions, wetting behaviour, roughness values and shape factor, which are in accordance with reportedly adequate ranges for biomedical applications.

Data availability

The raw/processed data required to reproduce these findings cannot be shared at this time due to time limitations and also to the fact that at this time this data also forms part of an ongoing study.

CRediT authorship contribution statement

Francisca Melo-Fonseca: Methodology, Investigation, Validation, Formal analysis, Writing – original draft, Funding acquisition. **Bruno Guimarães:** Methodology, Validation, Writing – review & editing. **Michael Gasik:** Writing – review & editing, Supervision, Funding acquisition. **Filipe S. Silva:** Conceptualization, Writing – review & editing, Supervision, Funding acquisition. **Georgina Miranda:** Conceptualization, Writing – review & editing, Supervision, Funding acquisition.

Declaration of Competing Interest

The authors declare that they have no known competing financial interests or personal relationships that could have appeared to influence the work reported in this paper.

Data Availability

The authors do not have permission to share data.

Acknowledgements

Supplementary materials

Supplementary material associated with this article can be found, in the online version, at doi:10.1016/j.surfin.2022.102466.

References

[1] M. Kaur, K. Singh, Review on titanium and titanium based alloys as biomaterials for orthopaedic applications, Mater. Sci. Eng. C. 102 (2019) 844–862, https://doi.org/10.1016/j.msec.2019.04.064.

[2] Q. Chen, G.A. Thouas, Metallic implant biomaterials, Mater. Sci. Eng. R 87 (2015) 1–57, https://doi.org/10.1016/j.mser.2014.10.001.

[3] M. Marian, R. Shah, B. Gashi, S. Zhang, K. Bhavnani, S. Wartzack, A. Rosenkranz, Exploring the lubrication mechanisms of synovial fluids for joint longevity – a perspective, Colloids Surf. B 206 (2021) 111926, https://doi.org/10.1016/j.colsurfb.2021.111926.

[4] M. Marian, D. Berman, N. Nečas, N. Emami, A. Ruggiero, A. Rosenkranz, Roadmap for 2D materials in biotribological/biomedical applications – a review, Adv. Colloid Interface Sci. 307 (2022), https://doi.org/10.1016/j.cis.2022.102747.

[5] R. Shah, B. Gashi, S. Hoque, M. Marian, A. Rosenkranz, Enhancing mechanical and biomedical properties of protheses - surface and material design, Surf. Interfaces 27 (2021), 101498, https://doi.org/10.1016/j.surfin.2021.101498.

[6] B.R. Sunil, A.S. Kranthi Kiran, S. Ramakrishna, Surface functionalized titanium with enhanced bioactivity and antimicrobial properties through surface engineering strategies for bone implant applications, Curr. Opin. Biomed. Eng. 23 (2022), 100398, https://doi.org/10.1016/j.cobme.2022.100398.

[7] N. Sirdeshmukh, G. Dongre, Laser micro & nano surface texturing for enhancing osseointegration and antimicrobial effect of biomaterials: a review, Mater. Today Proc. 44 (2021) 2348–2355, https://doi.org/10.1016/j.matpr.2020.12.433.

[8] T. Wang, L. Wang, Q. Lu, Z. Fan, Changes in the esthetic, physical, and biological properties of a titanium alloy abutment treated by anodic oxidation, J. Prosthet. Dent. 121 (2019) 156–165, https://doi.org/10.1016/j.prosdent.2018.03.024.

[9] F. Melo-Fonseca, M. Gasik, S. Madeira, F.S. Silva, G. Miranda, Surface characterization of titanium-based substrates for orthopaedic applications, Mater. Charact. 177 (2021), 111161, https://doi.org/10.1016/j.matchar.2021.111161.

[10] A. Henningsen, R. Smeets, P. Hartjen, O. Heinrich, R. Heuberger, M. Heiland, C. Precht, C. Cacaci, Photofunctionalization and non-thermal plasma activation of titanium surfaces, Clin. Oral Investig. 22 (2018) 1045–1054, https://doi.org/10.1007/s00784-017-2186-z.

[11] J.A. Wahab, M.J. Ghazali, W.M.W. Yusoff, Z. Sajuri, Enhancing material performance through laser surface texturing: a review, Trans. Inst. Met. Finish. 94 (2016) 193–198, https://doi.org/10.1080/00202967.2016.1191141.

[12] E. Martínez, E. Engel, J.A. Planell, J. Samitier, Effects of artificial micro- and nano-structured surfaces on cell behaviour, Ann. Anat. 191 (2009) 126–135, https://doi.org/10.1016/j.aanat.2008.05.006.

[13] A.O. Ijaola, E.A. Bamidele, C.J. Akisin, I.T. Bello, A.T. Oyatobo, A. Abdulkareem, P.K. Farayibi, E. Asmatulu, Wettability transition for laser textured surfaces: a comprehensive review, Surf. Interfaces 21 (2020), 100802, https://doi.org/10.1016/j.surfin.2020.100802.

[14] L.A. Turner, M.J. Dalby, Nanotopography-potential relevance in the stem cell niche, Biomater. Sci. 2 (2014) 1574–1594, https://doi.org/10.1039/c4bm00155a.

[15] F. Melo-Fonseca, G. Miranda, H.S. Domingues, I.M. Pinto, M. Gasik, F.S. Silva, Reengineering bone-implant interfaces for improved mechanotransduction and clinical outcomes, Stem Cell Rev. Rep. (2020), https://doi.org/10.1007/s12015-020-10022-9.

[16] M. Vishnoi, P. Kumar, Q. Murtaza, Surface texturing techniques to enhance tribological performance: a review, Surfa. Interfaces 27 (2021), 101463, https://doi.org/10.1016/j.surfin.2021.101463.

[17] I. Shivakoti, G. Kibria, R. Cep, B.B. Pradhan, A. Sharma, Laser surface texturing for biomedical applications: a review, Coatings 11 (2021) 1–15, https://doi.org/10.3390/coatings11020124.

[18] Q. Ding, L. Wang, L. Hu, Tribology optimization by laser surface texturing: from bulk materials to surface coatings, Laser Surf. Eng. Process. Appl. (2015) 405–422, https://doi.org/10.1016/B978-1-78242-074-3.00016-7.

[19] A. Singh, D. Patel, J. Ramkumar, K. Balani, Micro-channels fabrication through pulsed Nd:YAG laser on Ti6Al4V, Nanotechnol. Better Living (2016), https://doi.org/10.3850/978-981-09-7519-7nbl16-rps-120, 120–120.

[20] G. Kibria, A. Sen, H.M. Tariq Aziz, B. Doloi, B. Bhattacharyya, Pulsed Nd:YAG Laser Surface Texturing of Pure Titanium Material, Springer, Singapore, 2018, https://doi.org/10.1007/978-981-10-8767-7_14.

[21] S. Chatterjee, S.S. Mahapatra, V. Bharadwaj, A. Choubey, B.N. Upadhyay, K.S. Bindra, Drilling of micro-holes on titanium alloy using pulsed Nd:YAG laser: parametric appraisal and prediction of performance characteristics, Proc. Inst. Mech. Eng. Part B 233 (2019) 1872–1889, https://doi.org/10.1177/0954405418805604.

[22] N. Mirhosseini, P.L. Crouse, M.J.J. Schmidth, L. Li, D. Garrod, Laser surface micro-texturing of Ti-6Al-4V substrates for improved cell integration, Appl. Surf. Sci. 253 (2007) 7738–7743, https://doi.org/10.1016/j.apsusc.2007.02.168.

[23] D.S. Patel, A. Singh, K. Balani, J. Ramkumar, Topographical effects of laser surface texturing on various time-dependent wetting regimes in Ti6Al4V, Surf. Coatings Technol. 349 (2018) 816–829, https://doi.org/10.1016/j.surfcoat.2018.05.032.

[24] J. Lawrence, L. Hao, H.R. Chew, On the correlation between Nd:YAG laser-induced wettability characteristics modification and osteoblast cell bioactivity on a titanium alloy, Surf. Coatings Technol. 200 (2006) 5581–5589, https://doi.org/10.1016/j.surfcoat.2005.07.107.

[25] V. Dumas, A. Rattner, L. Vico, E. Audouard, J.C. Dumas, P. Naisson, P. Bertrand, Multiscale grooved titanium processed with femtosecond laser influences mesenchymal stem cell morphology, adhesion, and matrix organization, J. Biomed. Mater. Res. Part A. 100 A (2012) 3108–3116, https://doi.org/10.1002/jbm.a.34239.

[26] M. Zhu, H. Ye, J. Fang, C. Zhong, J. Yao, J. Park, X. Lu, F. Ren, Engineering high-resolution micropatterns directly onto titanium with optimized contact guidance to promote osteogenic differentiation and bone regeneration, ACS Appl. Mater. Interfaces. 11 (2019) 43888–43901, https://doi.org/10.1021/acsami.9b16050.

[27] L. Tiainen, P. Abreu, M. Buciumeanu, F. Silva, M. Gasik, R. Serna Guerrero, O. Carvalho, Novel laser surface texturing for improved primary stability of

[28] titanium implants, J. Mech. Behav. Biomed. Mater. 98 (2019) 26–39, https://doi.org/10.1016/j.jmbbm.2019.04.052.

[28] A. Cunha, A.M. Elie, L. Plawinski, A.P. Serro, A.M. Botelho Do Rego, A. Almeida, M.C. Urdaci, M.C. Durrieu, R. Vilar, Femtosecond laser surface texturing of titanium as a method to reduce the adhesion of Staphylococcus aureus and biofilm formation, Appl. Surf. Sci. 360 (2016) 485–493, https://doi.org/10.1016/j.apsusc.2015.10.102.

[29] X. Luo, S. Yao, H. Zhang, M. Cai, W. Liu, R. Pan, C. Chen, X. Wang, L. Wang, M. Zhong, Biocompatible nano-ripples structured surfaces induced by femtosecond laser to rebel bacterial colonization and biofilm formation, Opt. Laser Technol. 124 (2020), 105973, https://doi.org/10.1016/j.optlastec.2019.105973.

[30] B. Mao, A. Siddaiah, Y. Liao, P.L. Menezes, Laser surface texturing and related techniques for enhancing tribological performance of engineering materials: a review, J. Manuf. Process. 53 (2020) 153–173, https://doi.org/10.1016/j.jmapro.2020.02.009.

[31] M. Marian, A. Almqvist, A. Rosenkranz, M. Fillon, Numerical micro-texture optimization for lubricated contacts—a critical discussion, Friction (2022), https://doi.org/10.1007/s40544-022-0609-6.

[32] A. Soveja, E. Cicală, D. Grevey, J.M. Jouvard, Optimisation of TA6V alloy surface laser texturing using an experimental design approach, Opt. Lasers Eng. 46 (2008) 671–678, https://doi.org/10.1016/j.optlaseng.2008.04.009.

[33] ISO 11146-1:2005(en) Lasers and Laser-Related Equipment — Test methods For Laser Beam Widths, Divergence Angles and Beam Propagation Ratios — Part 1: Stigmatic and Simple Astigmatic Beams, Geneva, Switzerland, n.d., 2005 https://www.iso.org/standard/33626.html.

[34] E.S. Gadelmawla, M.M. Koura, T.M.A. Maksoud, I.M. Elewa, H.H. Soliman, Roughness parameters, J. Mater. Process. Technol. 123 (2002) 133–145, https://doi.org/10.1016/S0924-0136(02)00060-2.

[35] B. Guimarães, C.M. Fernandes, D. Figueiredo, O. Carvalho, F.S. Silva, G. Miranda, Effect of laser surface texturing on the wettability of WC-Co cutting tools, Int. J. Adv. Manuf. Technol. 111 (2020) 1991–1999, https://doi.org/10.1007/s00170-020-06155-3.

[36] M. Bussoli, T. Desai, D. Batani, B. Gakovic, M. Trtica, Nd:YAG laser interaction with titanium implant surfaces for medical applications, Radiat. Eff. Defects Solids. 163 (2008) 349–356, https://doi.org/10.1080/10420150701777678.

[37] L. Convert, E. Bourillot, M. François, N. Pocholle, F. Baras, O. Politano, S. Costil, Laser textured titanium surface characterization, Appl. Surf. Sci. 586 (2022), 152807, https://doi.org/10.1016/j.apsusc.2022.152807.

[38] A. Sen, B. Doloi, B. Bhattacharyya, Experimental studies on fibre laser micro-machining of Ti-6Al-4V, in: 5th Int. 26th All India Manuf. Technol. Des. Res. Conf. (AIMTDR 2014), 2014, pp. 1–7.

[39] Z. Yu, G. Yang, W. Zhang, J. Hu, Investigating the effect of picosecond laser texturing on microstructure and biofunctionalization of titanium alloy, J. Mater. Process. Technol. 255 (2018) 129–136, https://doi.org/10.1016/j.jmatprotec.2017.12.009.

[40] C.G. Moura, O. Carvalho, L.M.V. Gonçalves, M.F. Cerqueira, R. Nascimento, F. Silva, Laser surface texturing of Ti-6Al-4V by nanosecond laser: surface characterization, Ti-oxide layer analysis and its electrical insulation performance, Mater. Sci. Eng. C 104 (2019), 109901, https://doi.org/10.1016/j.msec.2019.109901.

[41] K.-.Y. Law, H. Zhao, Surface Wetting: Characterization, Contact Angle, and Fundamentals, Springer International Publishing, Basel, Switzerland, 2016, https://doi.org/10.1007/978-3-319-25214-8.

[42] X. Wang, C. Fu, C. Zhang, Z. Qiu, B. Wang, A comprehensive review of wetting transition mechanism on the surfaces of microstructures from theory and testing methods, Materials (Basel) 15 (2022) 1–21, https://doi.org/10.3390/ma15144747.

[43] I.G. Simões, A.C. dos Reis, M.L. da Costa Valente, Analysis of the influence of surface treatment by high-power laser irradiation on the surface properties of titanium dental implants: a systematic review, J. Prosthet. Dent. (2021) 1–8, https://doi.org/10.1016/j.prosdent.2021.07.026.

[44] F. Rupp, L. Scheideler, J. Geis-Gerstorfer, Effect of heterogenic surfaces on contact angle hysteresis: dynamic contact angle analysis in material sciences, Chem. Eng. Technol. 25 (2002) 877–882, https://doi.org/10.1002/1521-4125(20020910)25:9<877::AID-CEAT877>3.0.CO;2-D.

[45] C. juan Yang, X. song Mei, Y. ling Tian, D. wei Zhang, Y. Li, X. ping Liu, Modification of wettability property of titanium by laser texturing, Int. J. Adv. Manuf. Technol. 87 (2016) 1663–1670, https://doi.org/10.1007/s00170-016-8601-9.

[46] Y. Wang, X. Zhao, C. Ke, X. Yu, R. Wang, Nanosecond laser fabrication of superhydrophobic Ti6Al4V surfaces assisted with different liquids, Colloids Interface Sci. Commun. 35 (2020), 100256, https://doi.org/10.1016/j.colcom.2020.100256.

[47] O. Raimbault, S. Benayoun, K. Anselme, C. Mauclair, T. Bourgade, A.M. Kietzig, P.L. Girard-Lauriault, S. Valette, C. Donnet, The effects of femtosecond laser-textured Ti-6Al-4V on wettability and cell response, Mater. Sci. Eng. C 69 (2016) 311–320, https://doi.org/10.1016/j.msec.2016.06.072.

[48] E. Chikarakara, S. Naher, D. Brabazon, High speed laser surface modification of Ti-6Al-4V, Surf. Coatings Technol. 206 (2012) 3223–3229, https://doi.org/10.1016/j.surfcoat.2012.01.010.

[49] E. Chikarakara, P. Fitzpatrick, E. Moore, T. Levingstone, L. Grehan, C. Higginbotham, M. Vázquez, K. Bagga, S. Naher, D. Brabazon, In vitro fibroblast and pre-osteoblastic cellular responses on laser surface modified Ti-6Al-4V, Biomed. Mater. 10 (2015) 15007, https://doi.org/10.1088/1748-6041/10/1/015007.

[50] S. Mukherjee, S. Dhara, P. Saha, Enhanced corrosion, tribocorrosion resistance and controllable osteogenic potential of stem cells on micro-rippled Ti6Al4V surfaces produced by pulsed laser remelting, J. Manuf. Process. 65 (2021) 119–133, https://doi.org/10.1016/j.jmapro.2021.03.023.

[51] K.T. Voisey, C.A. Scotchford, L. Martin, H.S. Gill, Effect of Q-switched laser surface texturing of titanium on osteoblast cell response, Phys. Procedia. 56 (2014) 1126–1135, https://doi.org/10.1016/j.phpro.2014.08.027.

[52] Q. Zheng, L. Mao, Y. Shi, W. Fu, Y. Hu, Biocompatibility of Ti-6Al-4V titanium alloy implants with laser microgrooved surfaces, Mater. Technol. 00 (2020) 1–10, https://doi.org/10.1080/10667857.2020.1816011.

[53] J. Mesquita-Guimarães, R. Detsch, A.C. Souza, B. Henriques, F.S. Silva, A. R. Boccaccini, O. Carvalho, Cell adhesion evaluation of laser-sintered HAp and 45S5 bioactive glass coatings on micro-textured zirconia surfaces using MC3T3-E1 osteoblast-like cells, Mater. Sci. Eng. C. 109 (2020), 110492, https://doi.org/10.1016/j.msec.2019.110492.

[54] K. Anselme, P. Davidson, A.M. Popa, M. Giazzon, M. Liley, L. Ploux, The interaction of cells and bacteria with surfaces structured at the nanometre scale, Acta Biomater 6 (2010) 3824–3846, https://doi.org/10.1016/j.actbio.2010.04.001.